Optics Communications 420 (2018) 116–121

Contents lists available at ScienceDirect

Optics Communications

journal homepage: www.elsevier.com/locate/optcom

Compensation of carrier lifetime in double-pass semiconductor optical amplifiers

O.M. Kharraz [a,*], A.S.M. Supa'at [a], M.A. Mahdi [b]

[a] Department of Communication Engineering, Faculty of Electrical Engineering, Universiti Teknologi Malaysia, 81310 Skudai, Johor, Malaysia
[b] Wireless and Photonic Network Research Centre, Faculty of Engineering, Universiti Putra Malaysia, 43400 UPM Serdang, Selangor, Malaysia

ARTICLE INFO

Keywords:
Carrier lifetime
Double-pass
Four-wave mixing
Semiconductor optical amplifier
Unsaturated gain

ABSTRACT

Bi-directional light propagation is expected to enable enhanced functionality of all-optical signal processing operations compared to unidirectional approaches. In this work, we report on compensation of slow gain recovery in semiconductor optical amplifiers (SOAs) in a double-pass condition. The unsaturated gain of the employed SOA is increased by 12.6 dB, and the corresponding normalized conjugate output of four-wave mixing is enhanced by 16.3 dB. The theory attributes this efficiency improvement to the unsaturated gain enlargement which, in turn, compensates for the inherently long carrier lifetimes of SOAs by 50%. The saturation output power remains virtually unchanged.

1. Introduction

Semiconductor optical amplifiers (SOAs) are foreseen to be of potential and promising significance for low-cost fulfillment of high capacity and regenerative transmission in all-optical signal processing networks [1]. This is especially true, given recent progress in quantum-dots (QDs) technology, which has led to the development of QD SOAs possessing excellent features; ultra-fast gain recovery [2], ultra-wideband gain [3], low-noise figure [4], high saturation output power [5] and high four-wave mixing (FWM) efficiency [6]. FWM is a suitable technique to extract information on carrier mechanisms and characteristic times of the SOA nonlinear saturation process. It is also an efficient technology which enables all-optical signal processing functions; such as channels demultiplexing, 3R regenerations and frequency and data format translations. The response time of the SOA determines the quality of performance in these applications.

All-optical signal processing technology is regarded to be a key solution in forthcoming high-speed photonic networks. However, the optical non-linearities of commercially available bulk and quantum-well (QW) SOAs are still limited by their relatively long non-linear response times — which, in turn, restricts their switching speeds compared to their counterpart QD SOAs [7]. Due to the slow recovery of their carrier density, as determined by the carrier lifetime, FWM conversion deficiency becomes a critical limitation for these devices to be used as wavelength converters. Several attempts have been made to overcome the slow gain recovery of conventional bulk and QW SOAs. For example, an external holding beam at the transparency point of SOAs has been used to shorten their gain recovery time [8–10]. However, this method requires very large and external optical powers, increases complexity, reduces the useful gain considerably and also leads to signal distortion and broadening. Moreover, doped QW and QD SOAs can be designed and fabricated to facilitate SOAs with fast recovery times [11–13]. Resonant modulation of external beam injection has also brought about interesting features for cavity solitons response to overcome the slow carrier lifetime of semiconductor devices [14,15].

Whilst the aforementioned works focused on carrier lifetime acceleration, it would have also been possible to overcome the slow carrier lifetimes of SOAs by ensuring high unsaturated gain at a given maximum drive current value. The maximum value of FWM efficiency is predicted to increase linearly with the unsaturated gain and with the square of the saturation output power of the amplifier, i.e. $\eta \propto G_o P_{sat}^2$. Hence, SOAs of high unsaturated gain and saturation output power are more desirable for achieving higher conversion efficiency. Therefore, a small increase in the unsaturated gain produces a large increase in the FWM efficiency. This has been previously proven by driving the SOAs at higher bias currents, which also resulted in saturation output power being respectively enhanced [16]. In this article, we propose a double-pass SOA configuration to compensate for the bulk SOAs slow recovery time. The scheme is fully capable to utilize the entire available carrier densities in SOAs. The unsaturated gain is improved greatly from 21 dB to 33.6 dB for a given maximum device bias current, and the

* Correspondence to: Lightwave Communication Research Group, Universiti Teknologi Malaysia, 81310 Johor, Malaysia.
E-mail address: osayd-pd@utm.my (O.M. Kharraz).

https://doi.org/10.1016/j.optcom.2018.03.053
Received 4 January 2018; Received in revised form 15 February 2018; Accepted 22 March 2018

normalized conjugate output is significantly enhanced by 16.3 dB. The results provide an alternative approach to overcome the FWM deficiency restricted by the inherently slow response time of SOAs. Section 2 specifies the characterizations of the SOA. The results and discussions are explained and analyzed in Section 3. Finally, a summary is given in Section 4.

2. Analytical, numerical and experimental SOA characterizations

The analytical equation presented in [17] is used to study the response characteristics of the employed SOA. The saturated gain G can be determined from the following equation by means of convergence analysis.

$$\alpha' ln\frac{G_o}{G} = ln\frac{1-\alpha'\left(1+\frac{P_t(0)}{P_{sat}}\right)}{1-\alpha'\left(1+\frac{GP_t(0)}{P_{sat}}\right)} \quad (1)$$

where, α' is the normalized waveguide loss coefficient, P_t is total input power, P_{sat} is the saturation power, G_o is the unsaturated gain and G is the saturated gain. A complete derivation of Eq. (1) can be found in [17]. The SOA gain responses to different total input powers are also simulated using the numerical model described in [18] and outlined in Appendix A.

The experimental set-ups of both single and double pass arrangements of the FWM effect are illustrated in Fig. 1(a, b). Tunable laser sources are used as both the pump and probe signals. The polarizations of both FWM inputs are controlled using two polarization controllers. The outputs are combined using a 90/10 coupler to control the pump–probe ratio between the FWM inputs, and sent through an isolator to block the backward amplified spontaneous emission (ASE) of employed bulk SOA. An optical spectrum analyzer is used to characterize the output of the SOA. In the double-pass scheme, two circulators are utilized to allow for bidirectional propagations and also function as isolators. Characterization of the SOA ASE output spectra at various bias currents is given in Fig. 2(a). The output power of the ASE increases while driving the SOA (Alphion SAS26p) at higher DC currents and the center wavelength of the ASE (small signal gain spectrum) shifts to shorter wavelength. The SOA gain responses to different total input powers that are calculated by using both the analytical [17] and numerical [18] models and compared to the experiment are shown in Fig. 2(b). The analytical model fitting parameters at 0.1 A drive current used to plot the figure are unsaturated gain G_o = 15.71 dB, α' = 0.1 used in [17], and P_{sat} = 4.27 dBm. The corresponding analytical G values are then obtained by solving Eq. (1). The evaluated numerical values of the gain responses were found by using the parameters given in Table 1. The experimental, numerical and analytical values are marked in red, green and yellow colors, respectively. An excellent agreement between the theory and the experiment is observed prior to saturation regime, despite a 2 dB offset between the simulation (fiber to fiber gain) and experimental (device gain) results which has been compensated in Fig. 2(b). In the numerical simulation, we used a typical internal coupling loss value of 1500 m^{-1} per unit length, due to coupling losses at the input and output of the SOA. The recorded data from the experiment deals with the device gain rather than fiber to fiber gain. Assuming a coupling loss of +1 dB per facet, the total device gain is offset by +2 dB. Another important note refers to the location of the peak gain. From a commercially available SOA in a system standpoint, a design strategy that yields a high saturation output power across the C-band is to locate the peak gain far from the operating point. As described in the Alphion SOA specifications, the device is designed to operate in the C-band although the peak gain is located at around 1470 nm. This important correction in the gain profile has been implemented in the material gain Eq. (A.5).

Assuming an average value for the carrier density and hence the material gain all along the SOA gain region is an acceptable approximation for low input signal power levels and short SOAs, usually with a length under 250 μm. However, this approximation is not valid for long SOAs (typically with a length over 1 mm) operating in saturation without inclusion of a saturation factor. The numerical simulation is used to confirm the validity of our analytical solution, in which the latter can be confidently used to further study the FWM effect in the employed SOA.

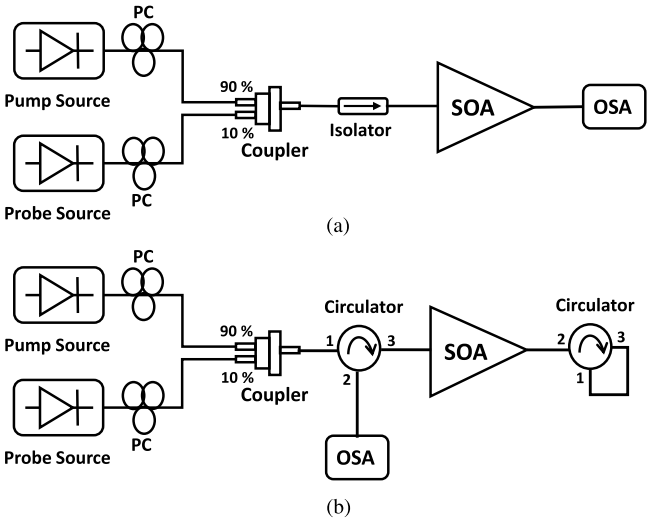

Fig. 1. Experimental set-ups of (a) single-pass, (b) double-pass configurations, in which PC: polarization controller, SOA: semiconductor optical amplifier, OSA: optical spectrum analyzer.

The total input power against the SOA gain responses at bias current of 550 mA in single-pass and double-pass configurations are drawn in Fig. 2(c). The theoretical and experimental single-pass results are shown in blue and red colors, while these are plotted in purple and green colors with the double-pass scheme, respectively. In the single pass scheme, the SOA has a small unsaturated gain G_o of 21 dB at input power of −40 dBm at 1548.31 nm wavelength with a P_{sat} of 10.3 dBm. The unsaturated gain is largely improved with the proposed double-pass set-up and increased to 33.6 dB, while the P_{sat} experiences no further change. The values of P_{sat} are obtained from Fig. 2(d). The path length of light circulating for one more time in the double-pass condition compared to the single-pass scheme has been implicitly compensated for in the theory by considering the experimental unsaturated gain values instead, which are directly dependent on the path length in the formula; $G_o = \exp\left[(\bar{g}-\alpha)L\right]$, where α is the gain factor related to the normalized waveguide loss coefficient, $\bar{g}$ is the unsaturated gain coefficient, L is the SOA length.

As can be seen in the figure, the analytical solution fits the experiment to a great extent at low power inputs, while it swerves at high power inputs due to the exclusion of spontaneous emission noise power in the model. The experimental performance of the SOA gain responses with respect to various output powers are shown in Fig. 2(d). The single pass results are plotted in red squares while the double-pass results are drawn in yellow triangles. The maximum polarization-dependent-gain between transverse electric and transverse magnetic components of the SOA-device is 1.5 dB at chip temperature of 25 °C at 550 mA-maximum operational drive current as specified in the data sheet.

3. Results and discussions

The impact of input power variations on normalized conjugate output and carrier lifetime of the SOA, in both single and double-pass configurations, is studied in Fig. 3(a). The normalized conjugate output (ρ) is defined as the power of the idler normalized to the output power of the probe, and given by:

$$\rho = \left|G'\right|^2 \exp\left\{Re\left[(1-j\alpha_l)\sigma F_{cd}(L,-\Omega)\right]\right\} \quad (2)$$

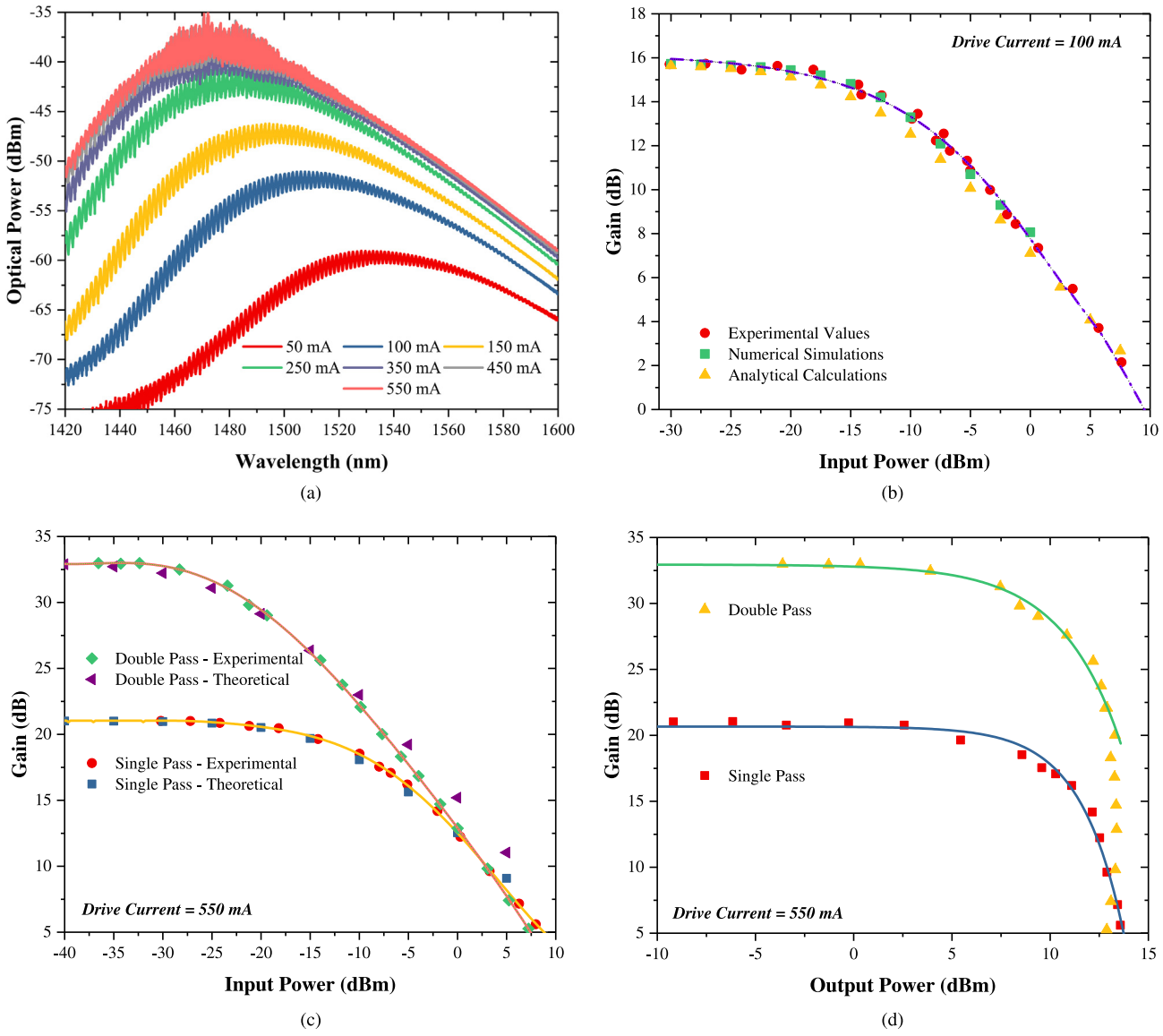

Fig. 2. (a) Measured ASE spectra at different operational currents, OSA resolution is 0.02 nm, (b) input power vs. SOA gain responses, bias current is 100 mA, (c) input power vs. SOA gain responses, bias current is 550 mA, (d) output power versus gain responses, SOA bias current is 550 mA. The center wavelength is 1548.31 nm. (For interpretation of the references to color in this figure legend, the reader is referred to the web version of this article.)

Table 1
List of parameter values used in the numerical simulation.

Symbol	Quantity (Units)	Values
a_m	Gain factor (m^2)	3×10^{-20}
c_1	Linear non-radiative recombination coefficient (s^{-1})	1.5×10^{8}
c_2	Bimolecular radiative recombination coefficient (m^3s^{-1})	10×10^{-17}
c_3	Auger recombination coefficient (m^3s^{-1})	3×10^{-41}
d	Active layer thickness (μm)	0.25
L	Amplifier length (mm)	1
L_m	Section length (mm)	0.1
n	Number of sections	10
n_e	Effective index	3.45
n_r	refractive index	3.4
n_g	Group index	3.56
N_o	Carrier density at transparency (m^{-3})	1×10^{24}
N_r	Reference carrier density (m^{-3})	3×10^{24}
W	Active region width (μm)	3
α_{in}	Internal loss (m^{-1})	1500
$\partial\omega_p/\partial N$	Frequency shift coefficient (m^3s^{-1})	2.12×10^{-11}
γ	Gain factor ($m^{-1}s^{-2}$)	2.7×10^{-24}
Γ	Confinement factor	0.3
ω_{p0}	Gain peak frequency (rad/s)	1.218×10^{15}
τ_s	Spontaneous carrier lifetime (ps)	400, I = 100 mA

where; G' is found from Eq. (B.1), α_l is the Henry's linewidth enhancement factor, σ is a proportionality constant, F_{cd} represent the contributions of carrier density modulation to the FWM response, L is the amplifier length and Ω is the beating frequency. The ρ values were calculated using the theoretical model described in [17,19] and defined in Appendix B with the fitting non-linear parameters detailed in Table 2. In the double-pass condition, there are two consequences to be considered when light circulate twice inside the amplifier. First, light path which has been compensated for by substituting the experimental double-pass unsaturated gain values in the models equations and second, time constants which are extracted from the model equations by fitting the experimental double-pass FWM results.

As can be depicted from the figure, double-pass arrangement enhances the ρ significantly by 15.32 dB and 6.26 dB, at input power of −16.1 dBm and 4.1 dBm, respectively, compared to single pass configuration, at 1.09 nm detuning bandwidth between probe signal and idler wavelengths. As the input power increases, the carrier lifetime of the SOA reduces with both single and double configurations. The SOA carrier lifetime is accelerated about two times — from 230 ps to 120 ps with the double-pass arrangement at low input power of −16.1 dBm, compared to single pass configuration. The advantage of double-pass set-up can also be gained at high input power, in which high ρ can be achieved due to the high unsaturated again attained with double-pass and consequently the carrier lifetime of SOAs is compensated. The latter is of an important interest where SOAs with slow gain recoveries can still be used to achieve high efficiencies in double-pass configurations. However, ρ decreases at high input power of around 7 dBm due to the amplifier operating in deep saturation whereby the carrier lifetime is found to increase.

Fig. 3(b) describes the relationship between the unsaturated gain of the employed SOA and ρ at detuning bandwidth of 1.95 nm and two different input powers of −16.1 dBm and 4.1 dBm for both single and double pass conditions. The applied bias current on the amplifier is increased to determine the maximum possible unsaturated gain that can be attained in single pass condition. At this point, the double-pass configuration is introduced with the drive current of the SOA set to maximum. The result of double pass is circled in blue-dotted circles in Fig. 3(b). At both input powers, the ρ grows linearly as the bias current is increased (unsaturated gain) [16] which also leads to quick recoveries of SOA carrier lifetimes [20]. At low input power of −16.1 dBm, double-pass configuration enlarges the unsaturated gain by 12.6 dB with bias current kept unchanged, enhances the ρ by 16.3 dB and also accelerates the carrier lifetime of the SOA in double. At larger input power of 4.1 dBm, the ρ is improved by 6.9 dB – by enlarging the unsaturated gain from 21 to 33.6 dB – with the double-pass configuration compared to the single pass, whereby the SOA carrier lifetime is compensated. Therefore, SOAs which possess high unsaturated gain are found to attain high efficiencies even though when their carrier lifetimes are inherently slow. That is to say, slow gain recovery SOAs can still be dealt with and considered for all-optical signal processing functions as far as double-pass arrangement is concerned.

The ρ variations across wide detuning bandwidths of 23 nm are plotted in Fig. 3(c) and (d), at input powers of −16.1 dBm and 4.1 dBm, respectively. The center wavelength of the pump is fixed at 1548.5 nm, while the probe signal wavelength is varied between 1548.9 to 1559.9 nm. The unsaturated gain is improved from 8.7 dB to 21 dB by varying the bias current of the SOA from 50 mA to 550 mA with the single pass arrangement, while it is enlarged to 33.6 dB with double-pass configuration. As can be perceived from both graphs, at a bandwidth detuning of ~21.5 nm, double pass condition improves the ρ by 13.9 dB and 6.6 dB, at input power of −16.1 dBm and 4.1 dBm, respectively. However, the improvement in the ρ at narrow detuning is higher than that at wide detuning bandwidths, due to polarization matching and efficient saturation being attained at closer detuning span between probe and idler wavelengths.

4. Summary

A double-pass SOA configuration has been experimentally demonstrated to compensate for the slow carrier lifetimes of bulk SOAs, enabling enhanced all-optical signal processing functionalities. The unsaturated SOA gain increased significantly, and the corresponding normalized conjugate output improved, while the saturation output power experienced almost no change. Theory was used to investigate the dynamic enhancement of SOA and to analyze the experimental FWM results. It has been found that the slow recovery time can be compensated by 50%, and the FWM deficiency can be consequently overcome. The unsaturated gain is improved from 21 dB to 33.6 dB for a given maximum device bias current, and the normalized conjugate output is enhanced by 16.3 dB.

Acknowledgments

The authors would like to acknowledge Universiti Teknologi Malaysia for funding this research under the post-doctoral fellowship scheme: Q.J130000.21A2.04E06 and the Royal Society-Newton-Ungku Omar Advanced Fellowship: NA150463.

Appendix A

In the simulation, the SOA length of 1 mm is virtually divided into 10 equal length sections. An ordinary rate equation is used to describe the carrier density of the mth section (N_m) along the SOA:

$$\frac{dN_m}{dt} = \frac{I_m}{qV_m} - R\left(N_m\right) - \frac{c}{n_g}\left[g\left(\omega, N_m\right) S_{m,sig} + \alpha_m\left(N_m - N_o\right) S_{m,spont}\right] \quad (A.1)$$

where the first term on the right-hand side represents the carriers (electrons) supply due to bias current in which I_m is the drive current of section m, q is the electron charge and V_m is the volume of the gain active region of section m. The second term represents the carrier consumption due to spontaneous carrier recombination, which is given as:

$$R(N) = c_1 N + c_2 N^2 + c_3 N^3 \quad (A.2)$$

here, c_1, c_2, and c_3 are constants where c_1 represents the non-radiative coefficient due to recombination at defects and traps, c_2 accounts for the spontaneous radiative recombination coefficient, and c_3 is the Auger recombination coefficient. $c_3 N^3$ represents the main non-radiative recombination process. The last term in Eq. (A.1) accounts for the carrier consumption due to stimulated emission, where S_{sig} and S_{spont} are the average photon densities of the signal and amplified spontaneous emission noise, respectively. n_g is the group refractive index, ω is the input signal frequency, α_m is the material gain factor and N_o is the carrier density at transparency. The rate equation is solved to obtain the time domain evolution of the input field at a certain position z along the SOA gain material. The average photon density for the amplified signal is given as:

$$S_{m,sig} = \frac{G_{s,m} - 1}{\ln\left(G_{s,m}\right)} \frac{\pi n_g}{c\zeta h\omega} \frac{2P_{in}\zeta\Gamma}{Wd} \quad (A.3)$$

where h is Planck's constant, and $\zeta = \sqrt{\mu_o/\epsilon_o}/n_e$ is the impedance of wave where μ_o is the vacuum permeability and ϵ_o is the vacuum permittivity, n_e is the effective index, Γ is the confinement factor which represents the fundamental waveguide mode intensity, W is the active layer width, and d is the active layer thickness. The total amplification experienced by the signal electric field for a medium of length L at a distance z from the input facet of the SOA amplifier is normally referred to as the amplifier single-pass gain. The signal gain is computed as:

$$G_{s,m}(z) = \exp\left[\Gamma\left(g\left(\omega, N_m\right) - \alpha_{in}\right) L_m\right] \quad (A.4)$$

Table 2
List of nonlinear fitting parameter values used in the analytical calculations, input power is ~7.1 dBm.

Symbol	Quantity (Units)	Values (Single Pass)	Values (Double-Pass)
τ	Carrier lifetime (ps)	48	79
τ_1	Hole burning time (fs)	24	40
τ_2	Carrier heating time (fs)	111	182
ε_{sh}	Hole burning parameter (mW^{-1})	16×10^{-3}	
ε_{ch}	Carrier heating parameter (mW^{-1})	4×10^{-3}	
α_l	Henry's linewidth enhancement factor	6	

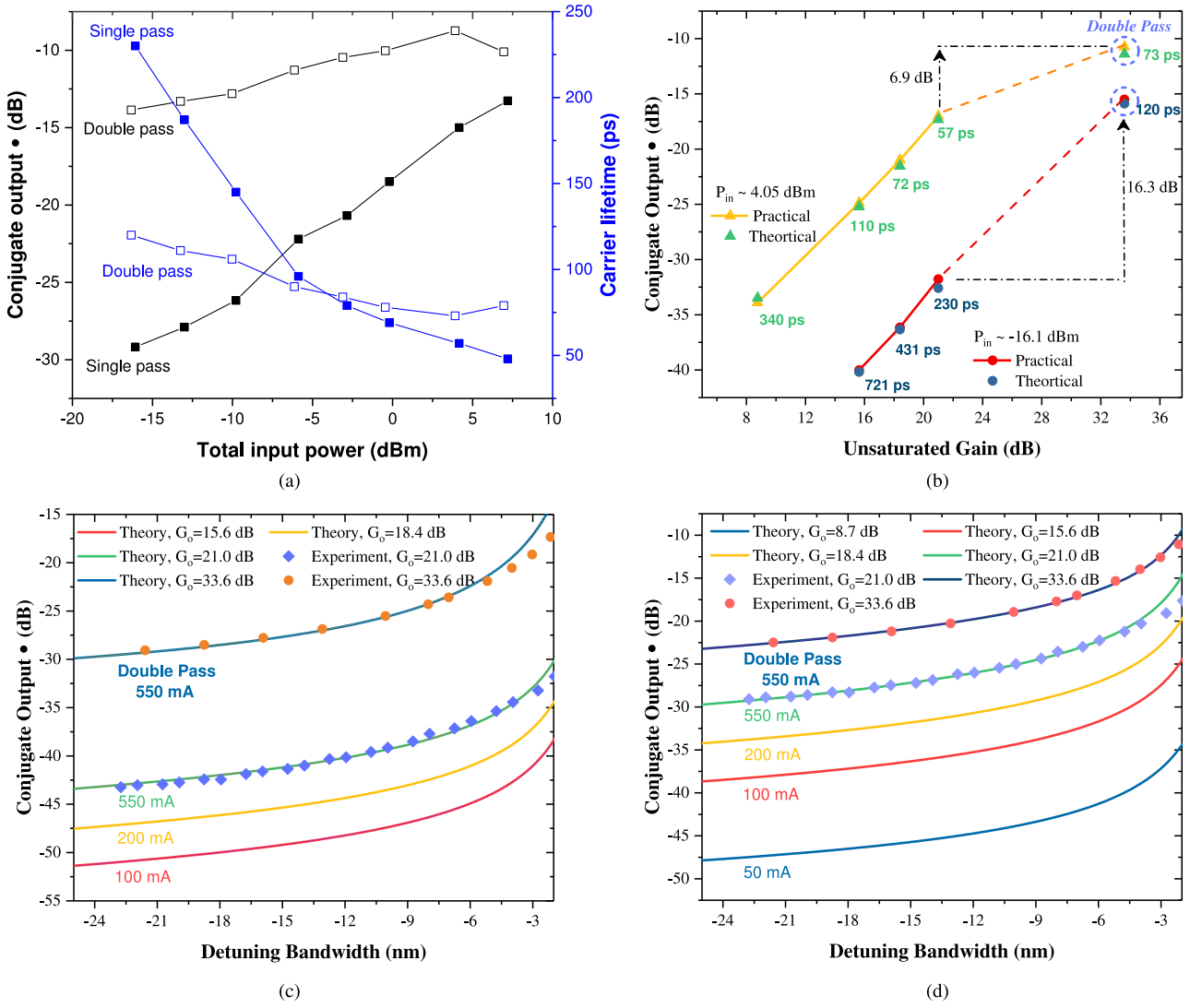

Fig. 3. (a) Total input power vs. conjugate output and carrier lifetime for both single and double-pass conditions, detuning bandwidth is 1.1 nm, (b) unsaturated gain vs. conjugate output and carrier lifetime, detuning bandwidth is 1.95 nm, (c) detuning bandwidth vs. conjugate output at input power of −16.1 dBm and (d) 4.16 dBm, drive current is 550 mA and pump–probe ratio is 12.8 dB.

where the carrier density can be numerically obtained from the rate equation and α_{in} is the internal loss per unit length. In the classical gain models, the material gain is phenomenologically expressed as:

$$g\left(\omega, N_m\right) = a_m\left(N_m - N_o\right) - \gamma\left(\omega - \omega_p\left(N_m\right)\right)^2 \tag{A.5}$$

where a_m and γ are both gain constants, N_o is the carrier density at transparency and ω_p is the peak wavelength. The first expression on the right-hand side represents the linear relation between the material gain and the carrier density due to injected current, whereas the second term provides the spectral profile and bandwidth of the gain. The signal peak wavelength is expected to move linearly with the carrier density:

$$\omega_p\left(N_m\right) = \omega_{p0} + \frac{\partial \omega_p}{\partial N}\left(N_m - N_r\right) \tag{A.6}$$

where ω_{p0} is the peak gain radian frequency at the reference carrier density N_r, and the constant $\frac{\partial \omega_p}{\partial N}$ is the radian frequency shift coefficient representing the peak frequency shift due to band filling effects with the carrier density N_m.

Appendix B

In this appendix, the detailed equations substituted in Eq. (2) and used to extract the non-linear parameters of SOA are given by:

$$G' = -\frac{1 - i\alpha_l}{\alpha_l}\exp\left[-\frac{1}{2}\sigma F_{cd}(\Omega)\right]\sin\left[\frac{\alpha_l}{2}\sigma F_{cd}(\Omega)\right] - \frac{1}{2}\varepsilon_{sh}P_{sat}H_{sh}(\Omega)\sigma F_{sh} - \frac{1}{2}\frac{g_o}{\bar{g}}\varepsilon_{ch}P_{sat}H_{ch}(\Omega)\sigma F_{ch} \tag{B.1}$$

$$F_{cd}(\Omega) = \frac{1}{1 - i\Omega\tau\alpha'}\left[\ln\left(\frac{1 + \frac{GP_t(0)}{P_{sat}} - i\Omega\tau}{1 + \frac{P_t(0)}{P_{sat}} - i\Omega\tau}\right) + \alpha'\ln\left(\frac{G_O}{G}\right)\right] \quad \text{(B.2)}$$

$$F_{sh} = \ln\left(\frac{G_O}{G}\right) \quad \text{(B.3)}$$

$$F_{ch} = -\frac{1}{\alpha'}\left[\frac{P_t(0)}{P_{sat}}(G-1) - \ln\left(\frac{G_O}{G}\right)\right] \quad \text{(B.4)}$$

$$P_t(0) = P_{sat}\left(\frac{1-\alpha'}{\alpha'}\right)\frac{1 - (\frac{G}{G_O})^{\alpha'}}{G - (\frac{G}{G_O})^{\alpha'}} \quad \text{(B.5)}$$

$$\sigma = \frac{P_O(0)}{P_O(0) - P_1(0)} \quad \text{(B.6)}$$

where; G is the saturated small signal gain, F_{α_l} represent the contributions of Henry's linewidth enhancement factor, Ω is the beating frequency, α' is the normalized waveguide loss coefficient, F_{sh} and F_{ch} represent the contributions of spectral hole burning and carrier heating to the FWM response, respectively, P_{sat} is the saturation power, P_t is the total power input, $\bar{g}$ is the unsaturated gain coefficient, g_o is the normalization gain, ϵ_{sh} and ϵ_{ch} are the strengths of the corresponding carrier heating (CH) and spectral hole burning (SHB) non-linear effects respectively, $P_O(0)$ and $P_1(0)$ are the average input powers of probe and pump elements correspondingly, τ is the spontaneous carrier lifetime, H_{ch} and H_{sh} are the Fourier transforms of the non-linear gain response due to CH and SHB respectively. These Fourier transforms are given by:

$$H_{ch}(\Omega) = \frac{1}{(1 - i\Omega\tau_1)(1 - i\Omega\tau_2)} \quad \text{(B.7)}$$

$$H_{sh}(\Omega) = \frac{1}{1 - i\Omega\tau_2} \quad \text{(B.8)}$$

where τ_1 is the characteristic time of the carrier-longitudinal optical phonon scattering that is responsible for in the cooling of the carrier distribution to the lattice temperature, and τ_2 is the characteristic time of the carrier–carrier scattering that is responsible for the filling of the hole burned by the field in the intra-band carrier distribution and also for the heating of the electron and hole gas.

References

[1] K.E. Stubkjaer, Semiconductor optical amplifier-based all-optical gates for high-speed optical processing, IEEE J. Sel. Top. Quantum Electron. 6 (2000) 1428–1435.

[2] N. Majer, K. Lüdge, E. Schöll, Cascading enables ultrafast gain recovery dynamics of quantum dot semiconductor optical amplifiers, Phys. Rev. B 82 (2010) 235301.

[3] T. Akiyama, M. Ekawa, M. Sugawara, H. Sudo, K. Kawaguchi, A. Kuramata, An ultrawide-band (120 nm) semiconductor optical amplifier having an extremely-high penalty-free output power of 23 dBm realized with quantum-dot active layers, in: Optical Fiber Communication Conference, Los Angeles, California, 2004, p. PD12.

[4] T.W. Berg, J. Mork, Saturation and noise properties of quantum-dot optical amplifiers, IEEE J. Quantum Electron. 40 (2004) 1527–1539.

[5] M. Sugawara, T. Akiyama, N. Hatori, Y. Nakata, H. Ebe, H. Ishikawa, Quantum-dot semiconductor optical amplifiers for high-bit-rate signal processing up to 160 Gb s -1 and a new scheme of 3R regenerators, Meas. Sci. Technol. 13 (2002) 1683.

[6] T. Akiyama, H. Kuwatsuka, N. Hatori, Y. Nakata, H. Ebe, M. Sugawara, Symmetric highly efficient (/spl sim/0 db) wavelength conversion based on four-wave mixing in quantum dot optical amplifiers, IEEE Photonics Technol. Lett. 14 (2002) 1139–1141.

[7] A.J. Zilkie, J. Meier, M. Mojahedi, P.J. Poole, P. Barrios, D. Poitras, et al., Carrier dynamics of quantum-dot, quantum-dash, and quantum-well semiconductor optical amplifiers operating at 1.55 μm, IEEE J. Quantum Electron. 43 (2007) 982–991.

[8] F. Ginovart, M. Amaya, A. Sharaiha, Semiconductor optical amplifier studies under optical injection at the transparency wavelength in copropagative configuration, J. Lightwave Technol. 25 (2007) 840–849.

[9] J.L. Pleumeekers, M. Kauer, K. Dreyer, C. Burrus, A.G. Dentai, S. Shunk, et al., Acceleration of gain recovery in semiconductor optical amplifiers by optical injection near transparency wavelength, IEEE Photonics Technol. Lett. 14 (2002) 12–14.

[10] V. Nithin, Y. Kumar, M.R. Shenoy, Novel scheme of assist-light injection through waveguide coupling in a semiconductor optical amplifier for fast gain recovery, Opt. Commun. 359 (2016) 419–425.

[11] M. Sugawara, N. Hatori, M. Ishida, H. Ebe, Y. Arakawa, T. Akiyama, et al., Recent progress in self-assembled quantum-dot optical devices for optical telecommunication: temperature-insensitive 10 Gb s −1 directly modulated lasers and 40 Gb s −1 signal-regenerative amplifiers, J. Phys. D: Appl. Phys. 38 (2005) 2126.

[12] A.J. Zilkie, J. Meier, P.W.E. Smith, M. Mojahedi, J.S. Aitchison, P.J. Poole, et al., Femtosecond gain and index dynamics in an InAs/InGaAsP quantum dot amplifier operating at 1.55 μm, Opt. Express 14 (2006) 11453–11459.

[13] M.N. Ngo, G. Girault, M. Gay, L. Bramerie, J.-C. Simon, R. Brenot, et al., Suppression of slow gain recovery in ultralong quantum-dash semiconductor optical amplifier emitting at 1.55μm, Opt. Commun. 284 (2011) 4910–4913.

[14] S. Ahmadipanah, R. Kheradmand, F. Prati, Enhanced resonance frequency and modulation bandwidth in a cavity soliton laser, IEEE Photonics Technol. Lett. 26 (2014) 1038–1041.

[15] M. Eslami, R. Kheradmand, High bit-rate cavity soliton-based differential phase-shift-keying demodulator, J. Modern Opt. 61 (2014) 116–121.

[16] A. D'Ottavi, A. Mecozzi, S. Scotti, F.C. Romeo, F. Martelli, P. Spano, et al., Four-wave mixing efficiency in traveling wave semiconductor optical amplifiers at high saturation, Appl. Phys. Lett. 67 (1995) 2753–2755.

[17] A. Mecozzi, S. Scotti, A.D. Ottavi, E. Iannone, P. Spano, Four-wave mixing in traveling-wave semiconductor amplifiers, IEEE J. Quantum Electron. 31 (1995) 689–699.

[18] T. Durhuus, B. Mikkelsen, K.E. Stubkjaer, Detailed dynamic model for semiconductor optical amplifiers and their crosstalk and intermodulation distortion, J. Lightwave Technol. 10 (1992) 1056–1065.

[19] O.M. Kharraz, A.B.B. Mohammad, D.I. Forsyth, A.A. Jasim, H. Ahmad, Polarization-independent ASE four-wave mixing in a fast semiconductor optical amplifier, Opt. Commun. 355 (2015) 498–503.

[20] P. Berger, M. Alouini, J. Bourderionnet, F. Bretenaker, D. Dolfi, Dynamic saturation in semiconductor optical amplifiers: accurate model, role of carrier density, and slow light, Opt. Express 18 (2010) 685–693.